

DETC2008-49244

DYNAMIC MODELING OF A SLIDER-CRANK MECHANISM UNDER JOINT WEAR

Saad Mukras

Mechanical & Aerospace Eng.
University of Florida
Gainesville, FL 32611
mukras@ufl.edu

Nate Mauntler

Mechanical & Aerospace Eng.
University of Florida
Gainesville, FL 32611
mauntler@ufl.edu

Nam Ho Kim

Mechanical & Aerospace Eng.
University of Florida
Gainesville, FL 32611
nkim@ufl.edu

Tony Schmitz

Mechanical & Aerospace Eng.
University of Florida
Gainesville, FL 32611
tschmitz@ufl.edu

W. Gregory Sawyer

Mechanical & Aerospace Eng.
University of Florida
Gainesville, FL 32611
wgsawyer@ufl.edu

ABSTRACT

A study of how joint wear affects the kinematics of a simple slider-crank mechanism and in turn how change in kinematics of the mechanism affects the joint wear is presented. The coupling between joint wear and system kinematics is modeled by integrating a wear prediction process, built upon a widely used finite-element-based iterative scheme, with the dynamic model that has an imperfect joint whose kinematics changes progressively according to joint wear. Three different modeling techniques are presented based on different assumptions, and their performances are compared in terms of joint forces and wear depths. It turns out that the joint wear increases the joint force and accelerates the wear progress. The accuracy of integrated dynamic model is validated by measuring joint force and wear depth of the slider-crank mechanism. Details of instrumentation are also presented.

1. INTRODUCTION

Clearances at the joints of multibody systems (usually due to manufacturing tolerance) have been noted to affect the performance and service life of mechanical systems. This may be attributed to the dynamic force amplification as discussed by Dubowsky [1], increased vibration and excessive wear. Many studies on how joint clearance affects the response of multibody systems have been conducted, for example [1-10]. Although these studies will go a long way into allowing designer to take into account joint clearance, the findings may be limited to ideal case in which wear is assumed to be nonexistent. This is

because the studies have assumed that the clearance will remain the same throughout the service life of the system. This is contrary to a realistic scenario in which wear is expected to increase the clearance size. This research seeks to address this issue by allowing the joint clearance to vary as dictated by wear.

In the first part of the paper a wear prediction procedure is presented. The procedure presented is based on a widely used finite-element-based iterative wear prediction procedure but is improved so as to optimize the use of resources as wear is a computationally expensive analysis [11, 12]. In the next part, modeling of a perfect and imperfect joint is discussed. Two different kinds of imperfect joints are discussed. The first model is a simplified model in which the two components of the joint are in continuous contact. The second mode is more realistic in that the two components of the joint are allowed to move relative to each other depending on the dynamic behavior of the system. Next, the wear prediction procedure is integrated with the model that describes the imperfect joint. Only the continuous contact case is considered for the integration. In the final part of the paper the details of an instrumented slider-crank mechanism are presented. The slider-crank mechanism was built in order to verify the current study.

2. WEAR PREDICTION

In our previous studies [11], we used an Archard-type linear wear model to simulate the progressive wear in 3-D mechanical parts. The wear model describes the relationship between the wear rate and operating conditions:

$$\frac{dh}{ds} = K \cdot p \quad (1)$$

where h is the depth of recession of the material normal to the surface, s is the slip distance, K is the wear coefficient, and p is the contact pressure in the interface. If we consider the slip distance as an intrinsic time, then the above equation can be solved numerically, similar to the time integration in structural dynamics. In numerical integration, continuous time is discretized and the equilibrium condition is imposed in discrete steps. For example, the forward Euler method can be used to calculate

$$\Delta h_j = K \cdot p_j \cdot \Delta s_j, \quad (2)$$

where p_j is the contact pressure and Δs_j is the incremental slip distance at s_j . The total wear depth can then be updated by

$$h_j = h_{j-1} + \Delta h_j. \quad (3)$$

Numerical wear simulations calculate the wear depth by performing finite element analysis for a representative cycle and then extrapolating this wear depth over N fixed cycles. Extrapolation provides a solution to the computational cost problem but its use may introduce other problems. The accuracy and stability of the simulation may be lost by using extrapolation sizes that are too large. On the other hand using too small extrapolation sizes will result in a less than optimum use of resources. A complete study on extrapolations and its effect on stability of wear prediction can be found in the previous work [12].

3. DYNAMIC MODELING OF IMPERFECT JOINTS

In most wear tests and simulations, it is assumed that the operating condition is known and remains constant. In reality, however, wear of the contacting surfaces can change the kinematics of the system as well as the contact pressure distribution, resulting in changes in future wear patterns. In order to predict the service life of such a system, it is necessary to integrate wear prediction tools with system dynamic analysis. In this section, a computational method is developed to couple wear of the contacting surfaces with systems of evolving kinematics.

The slider-crank mechanism was selected to study this coupling phenomenon. A diagram of the slider-crank mechanism to be used in the study is shown in Figure 1. The study is simplified by eliminating friction and wear from all connecting points in the mechanisms except for one joint (shown as the joint of interest in Figure 1). This joint essentially consists of a hardened pin attached to the crank (drive-link) inside a softer bushing attached to the driven-link. A spring is attached to the slider which serves as a means to increase the joint reaction force and hence accelerated the wear occurring at the joint.

In order to successfully study the coupling phenomenon between the wear and kinematics evolution, it is necessary to develop a formulation for the slider-crank system that estimates the evolving kinematics and hence the joint reactions. In what follows, a formulation for the kinematic analysis of the slider-crank mechanism with perfect joints is presented. Based on this formulation, the formulation for the slider-crank mechanism with an imperfect joint will be developed. As a verification step for the correctness of the imperfect joint formulation, a comparison will be made between the kinematics of two models with the condition that no wear has occurred at the imperfect joint.

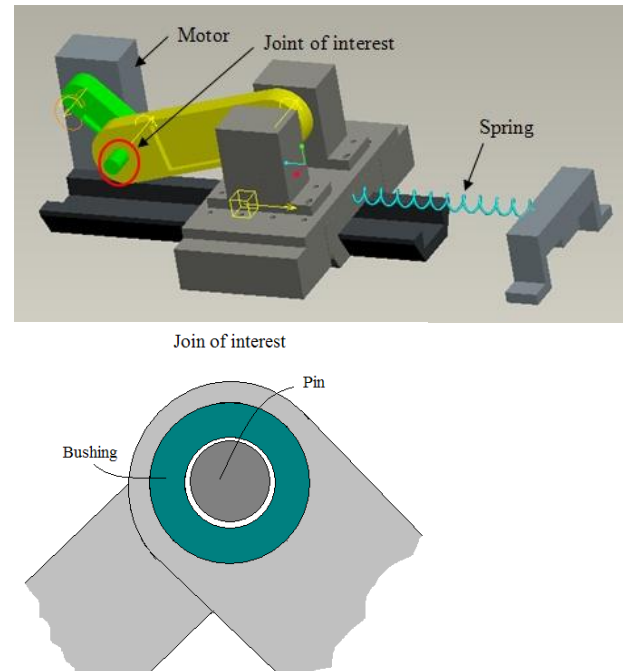


Figure 1 Slider-crank mechanisms to be used in the wear study.

3.1. Kinematics of Perfect Joints:

In slider-crank mechanism with perfect joint, the pin is assumed to fit perfectly in the bushing. Consequently the pin and bushing centers coincide at all times. The slider-crank system is assumed to consist of three rigid bodies with planar motion. Consider the diagram shown in Figure 2 in which the global Cartesian coordinate $x-y$ is used. The three disassembled components (link-1, link-2 and a slider) are shown in the global axis. Each component can translate and rotate in the plane.

The kinematics of the system is determined by imposing constraints on the motion of the components. These constraints result in a set of simultaneous equations that can be solved to reveal the overall system motion. With reference to Figure 2, the kinematics of the slider-crank mechanism can be described by ten nonlinear simultaneous constraint equations. The constraint equations are summarized as follows:

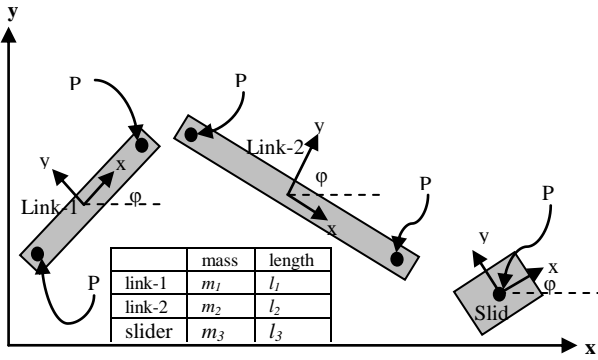


Figure 2 Components of the slide crank mechanisms.

$$\Phi = \begin{bmatrix} x_1 - l_1 \cos \phi_1 \\ y_1 - l_1 \sin \phi_1 \\ x_2 - 2l_1 \cos \phi_1 - l_2 \cos \phi_2 \\ y_2 - 2l_1 \sin \phi_1 - l_2 \sin \phi_2 \\ x_3 - 2l_1 \cos \phi_1 - 2l_2 \cos \phi_2 \\ y_3 - 2l_1 \sin \phi_1 - 2l_2 \sin \phi_2 \\ y_3 \\ \phi_3 \\ \phi_1 - \omega t \end{bmatrix} = \begin{bmatrix} 0 \\ 0 \\ 0 \\ 0 \\ 0 \\ 0 \\ 0 \\ 0 \\ 0 \end{bmatrix} \quad (4)$$

The first two constraints confine point P1 on link-1 to the origin. The next two constraints link points P1 and P2 using a perfect pin joint. These constraints will be relaxed in the later part of modeling. The next two constraints link points P4 and P5 using a perfect pin joint. The next two constraints make point P5 to remain on the x-axis without rotation. The final constraint, known as the driving constraint, is an external input such as a servo motor. For the current case a constant angular velocity is imposed in link-1.

It can be seen from the set of simultaneous equations above, that the number of equations exactly equals the number of unknowns. The unknowns are the DOFs of the components at the center of masses. This is denoted by vector \mathbf{q} , as

$$\mathbf{q} = [x_1, y_1, \phi_1, x_2, y_2, \phi_2, x_3, y_3, \phi_3]^T. \quad (5)$$

The above nonlinear equations can be solved simultaneously to determine the slider-crank mechanism component positions at any instant. The velocities and accelerations may also be determined using the following relations:

$$\dot{\mathbf{q}} = -\Phi_{\mathbf{q}}^{-1} \Phi_t \quad (6)$$

$$\ddot{\mathbf{q}} = -(\Phi_{\mathbf{q}} \dot{\mathbf{q}})_{\mathbf{q}} \dot{\mathbf{q}} - 2\Phi_{\mathbf{q}t} \dot{\mathbf{q}} - \Phi_{tt} \quad (7)$$

where $\Phi_{\mathbf{q}}$ and Φ_t are the Jacobian and time derivative of the constraints in Eq. (4). Once the accelerations have been computed, the reaction forces can be obtained through the process of reverse dynamics.

3.2. Kinematics of a Slider-Crank Mechanism with an Imperfect Joint:

Two cases of the imperfect joint are possible. In the first case, the contact between the two components of the joint, the pin and bushing, is considered to be continuous. That is, the pin contacts the bushing at only one location during the entire motion. We refer to this as continuous contact. In the second case the pin comes in contact with the bushing at different locations during the motion. Naturally, this case is referred to as non-continuous contact. In what follows only the imperfect joint with continuous contact is discussed. The case with non-continuous contact will be addressed later.

The slider-crank mechanism with the imperfect joint (continuous contact) is shown in Figure 3. This mechanism is identical to the previous one with the exception of the imperfect joint. As a result the constraints equations for both slider-crank mechanisms are similar except for the imperfect joint. Due to the similarity, only the constraint equation formulation for the imperfect joint will be presented.

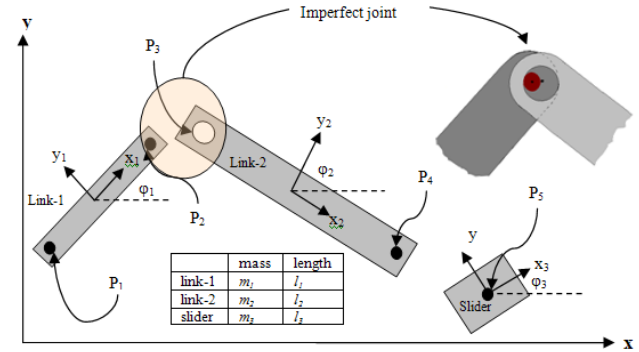


Figure 3 Disassembled slider-crank mechanisms with an imperfect joint.

In modeling the imperfect joint three assumptions are made. These include the following:

1. The pin (attached to link-1 necessary for the joint to be defined) is made of a hard material so that it does not experience any appreciable wear. The joint position of link-2 is fitted with a soft bushing (see Figure 4) that experiences considerable wear with only few cycles).
2. It is assumed that the pin will be in contact with the bushing at all the times. This assumption is due to the tension force provided by the spring attached to the slider.
3. It is also assumed that the point on the bushing where the pin first establishes contact with the bushing does not

change. This point is shown in Figure 4. It is the point that intersects the contact surface of the bushing with the line parallel to the local x-axis of *link-2* (as shown in Figure 3).

With these assumptions in place, the constraint equations relating to the imperfect joint can be derived with the aid of Figure 5. Note that an additional variable (α) is required in order to formulate the imperfect joint constraint, as is evident from Figure 5. The addition variable (α) describes the angle between the local x-axes of the two links. It also allows determination of the point of contact for the pin at any instant of the motion. This information will later be required to determine the relative slip distance between the pin and the bushing.

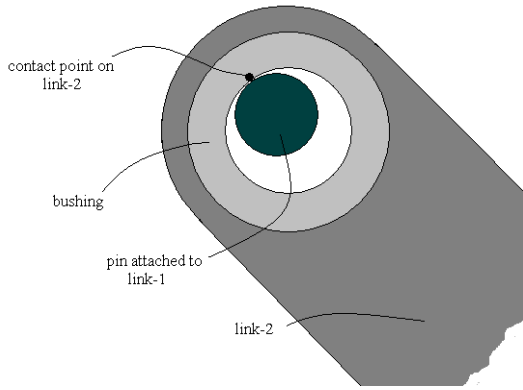


Figure 4 Imperfect joint consisting of a bushing and hardened pin.

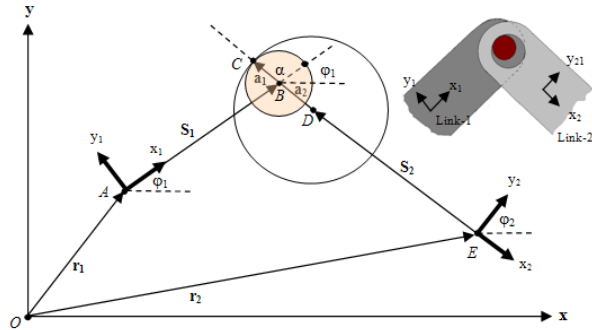


Figure 5 Kinematics of slider-crank mechanism with imperfect joint.

The imperfect joint constraints are formulated by imposing two conditions. These are described as below:

- Since the pin and bushing are assumed to be in contact at all times, a loop starting from the origin to the point of contact and back to the origin should be closed. In Figure 5 this loop is described by vectors that follow the path $O-A-B-C-D-E-O$. This loop can be represented mathematically as follows:

$$\mathbf{r}_1 + \mathbf{A}_1 \mathbf{s}_1 + \mathbf{A}_{11} \mathbf{a}_1 - \mathbf{A}_2 \mathbf{s}_2 - \mathbf{A}_2 \mathbf{a}_2 - \mathbf{r}_2 = \mathbf{0} \quad (8)$$

where \mathbf{A}_1 , \mathbf{A}_{11} and \mathbf{A}_2 are transformation matrices that transform the local vector \mathbf{s}_1 , \mathbf{a}_1 and \mathbf{s}_2 , and \mathbf{a}_2 into global vectors, respectively. The constraint equation can thus be written as follows:

$$\begin{bmatrix} -x_2 + 2l_1 \cos \phi_1 \\ +R_1 \cos(\phi_1 + \alpha) + [R_2 + l_2] \cos \phi_2 \\ -y_2 + 2l_1 \sin \phi_1 \\ +R_1 \sin(\phi_1 + \alpha) + [R_2 + l_2] \sin \phi_2 \end{bmatrix} = \begin{bmatrix} 0 \\ 0 \end{bmatrix} \quad (9)$$

where R_1 and R_2 are the radius of the pin and bushing respectively.

- The second constraint requires that the vector along the line $B-C$ and the vector along $D-C$, to be parallel. The vector along line $B-C$, expressed as $\mathbf{g}_1 = \mathbf{A}_{11} \mathbf{a}_1$, is the vector that runs from the center of the pin to the point of contact. It is noted that this vector, in both local and global coordinated systems, changes its orientation according to the variable α when the mechanism is in motion. On the other hand, the vector along line $D-C$, expressed as $\mathbf{g}_2 = \mathbf{A}_2 \mathbf{a}_2$, does not change its orientation in the local coordinate system of link-2. This is consistent with the third assumption that was earlier mentioned. The second requirement can be stated mathematically as follows:

$$\mathbf{g}_1^\perp \cdot \mathbf{g}_2 = 0 \quad (10)$$

This reduces to the following expression:

$$R_1 R_2 \sin(\phi_1 - \phi_2 + \alpha) = 0 \quad (11)$$

The two requirements mentioned above yield three constraint equations that describe the imperfect joint. The constraint equations for the other joints of the slider-crank mechanism with an imperfect joint can be formulated in the same manner as was described for the slider-crank mechanism with perfect joints. The constraint equations for the slider-crank mechanism with an imperfect joint can be summarized as follows:

$$\Phi = \begin{bmatrix} x_1 - l_1 \cos \phi_1 \\ y_1 - l_1 \sin \phi_1 \\ -x_2 + 2l_1 \cos \phi_1 + R_1 \cos(\phi_1 + \alpha) + [R_2 + l_2] \cos \phi_2 \\ -y_2 + 2l_1 \sin \phi_1 + R_1 \sin(\phi_1 + \alpha) + [R_2 + l_2] \sin \phi_2 \\ R_1 R_2 \sin(\phi_1 - \phi_2 + \alpha) = 0 \\ -x_3 + 2l_1 \cos \phi_1 + R_1 \cos(\phi_1 + \alpha) + [R_2 + 2l_2] \cos \phi_2 \\ -y_3 + 2l_1 \sin \phi_1 + R_1 \sin(\phi_1 + \alpha) + [R_2 + 2l_2] \sin \phi_2 \\ y_3 \\ \phi_3 \\ \phi_1 - \omega t \end{bmatrix} = \begin{bmatrix} 0 \\ 0 \\ 0 \\ 0 \\ 0 \\ 0 \\ 0 \\ 0 \\ 0 \\ 0 \end{bmatrix} \quad (12)$$

The set of simultaneous equations can once again be solved to determine the vector $\mathbf{q} = [x_1, y_1, \phi_1, x_2, y_2, \phi_2, x_3, y_3, \phi_3, \alpha]^T$

of the component of the mechanism with an imperfect joint. It should be noted that due to the additional variable α , an additional equation was required in order to solve the problem.

The Imperfect joint was formulated with variable radius for both the pin and bushing. For the current study, the pin is assumed to be made of a hard material so that it experiences negligible wear. As such the radius of the pin R_1 remains approximately constant. On the other hand the bushing is made of a softer material that will experience appreciable wear. It was assumed in the formulation of the imperfect joint that the point of contact on the bushing will not change. This assumption enables the simulation of the evolving kinematics (due to wear) by simply varying R_2 . Thus to represent wear, R_2 can be increased an amount equal to the worn-out material. The next stage of the study will involve integrating the wear simulation program with the evolving force estimation program for a real time update on the reaction force.

3.3. Verification of Imperfect Joint Formulation:

Before the model formulation for the slider-crank mechanism with an imperfect joint can be put to use, it is necessary to assess the adequacy of the model. One simple way to achieve this is to note that when $R_1 = R_2$ in the imperfect slider-crank model, the model reduced to the perfect joint slider-crank model. The correctness of the model can then be verified by comparing results from the two models. Since the imperfect slider-crank model is essentially the perfect slider-crank model when $R_1 = R_2$ it should be expected that the results will be identical.

The results from the kinematics analysis (position, velocity and acceleration) as well as the reverse dynamics analysis for two models are compared in Figure 6 through Figure 9. As was expected, the two models yielded identical results for the special case ($R_1 = R_2$). Although further verification will be provided using experimental results, it is concluded that the model formulation for the slider-crank mechanism with an imperfect joint is adequate enough to conduct the study of wear with kinematics evolution.

A plot of the changing reaction force as the gap between in the joint increases is shown in Figure 10. It is clear from the plot that the change in reaction force as the gap is increased is captured by the proposed imperfect joint formulation model for the slider-crank mechanism. Indeed further experimental tests are required to determine the accuracy of the model.

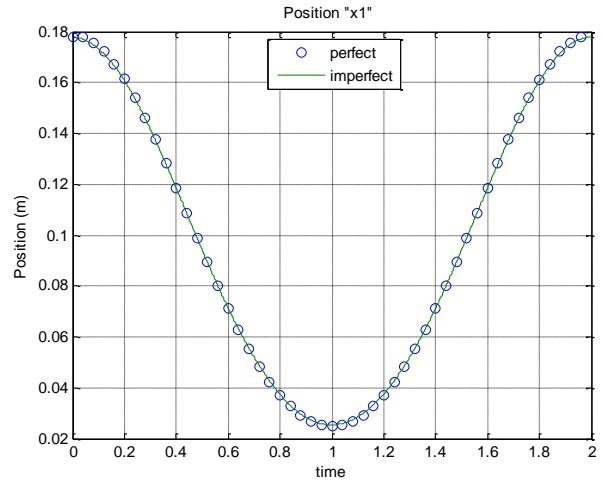


Figure 6 Comparison of x component of position of Link-1 for the perfect and imperfect joint models.

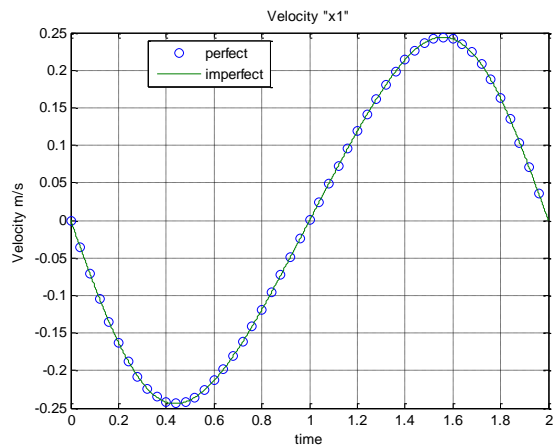


Figure 7 Comparison of x component of velocity of Link-1 for the perfect and imperfect joint models.

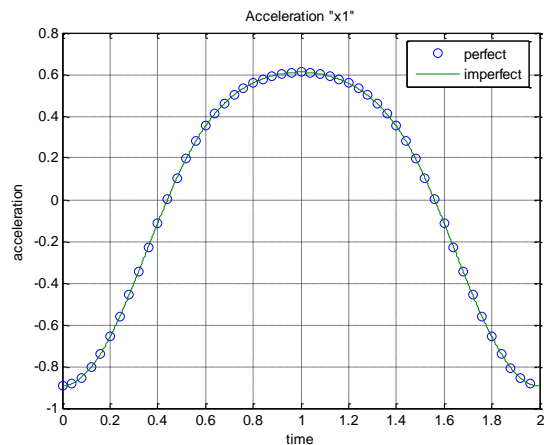


Figure 8 Comparison of x component of acceleration of Link-1 for the perfect and imperfect joint models.

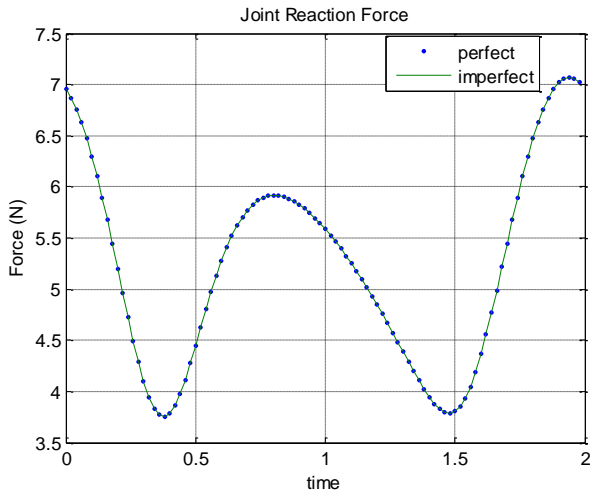


Figure 9 Comparison of reaction force at the joint between *link-1* and *link-2* for the perfect and imperfect joint models.

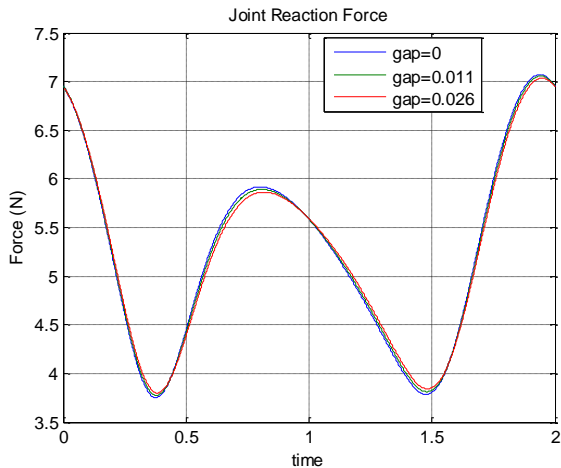


Figure 10 Change of the reaction force as the gap between in the joint increases

4. WEAR ANALYSIS OF SYSTEMS WITH KINEMATIC EVOLUTION:

It was shown in the previous section that inclusion of a clearance gap between the pin and bushing has an effect on the joint reaction force. It is therefore safe to conclude that wear at the joint would also alter the reaction force. In this section the effect of the wear on the reaction forces and in turn the effect of the changing reaction force on the wear will be studied. In order to achieve this, a two step procedure is proposed as illustrated in Figure 11. In the first stage a kinematic analysis is performed to determine the reaction forces and sliding distance between the two contacting components of the joint. In the next stage the reaction force and sliding distance is used to determine the wear at the joint. In what follows these stages will be discussed in more detail.

4.1. Kinematic analysis (determination of joint reaction force and sliding distance):

The procedure to determine the joint reaction forces has been discussed in Section 3 and will be left out in this section. In order to determine the relative motion or slip distance between the pin and bushing, it is assumed that the sliding distance will remain the same throughout the entire life of the slider-crank. This assumption is reasonable since the wear would cause a negligible change in the sliding distance.

The slip distance for an entire cycle is determined by selecting a reference point on the pin as well as on the bushing as shown in Figure 12. The angle difference between these reference points is measured as the crank completes a cycle.

At incremental rotation of the complete cycle, the angle difference is recorded. The slip angle is then determined as the angle difference between two adjacent data points. The slip distance can then be determined based on the diameter of the pin and the slip angles. Figure 13 shows an example of the slip distance during a complete cycle of the slider-crank system.

The reaction forces and the sliding distance obtained from the kinematic analysis can then be used for the wear analysis. This is discussed in the next section.

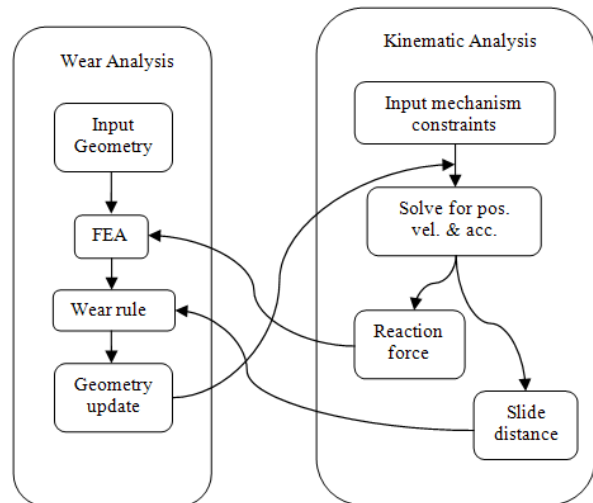


Figure 11 Analysis of systems with kinematic evolution

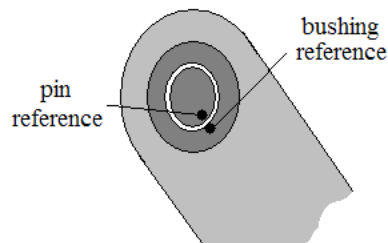


Figure 12 Pin and bushing reference points.

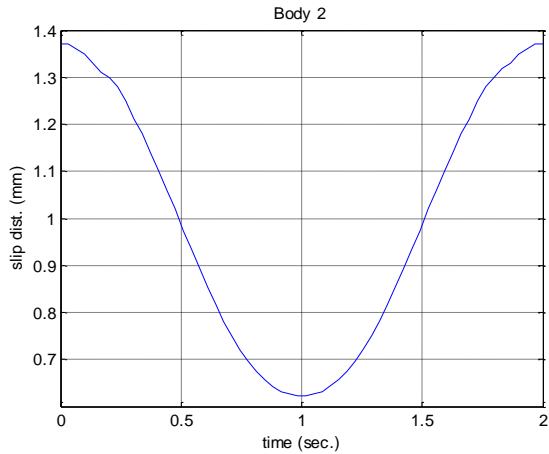


Figure 13 Sliding/slip distance at the joint for a complete crank cycle.

4.2. Wear analysis of a slider-crank mechanism with an imperfect joint (continuous contact):

For the wear analysis, the slip distance and the joint force for each cycle are determined in the same manner as described in the previous section. In order to calculate the wear at the joint, both the pin and bushing is isolated from the rest of the system. As mentioned earlier, the pin is taken to be hard enough so that it does not deform and no appreciable wear occurs on it. It can thus be modeled as a rigid body. This assumption was made so as to reduce the complexity of the analysis. On the other hand the bushing can deform and wear. The suggested finite element model for the pin and bushing assembly is shown in Figure 14.

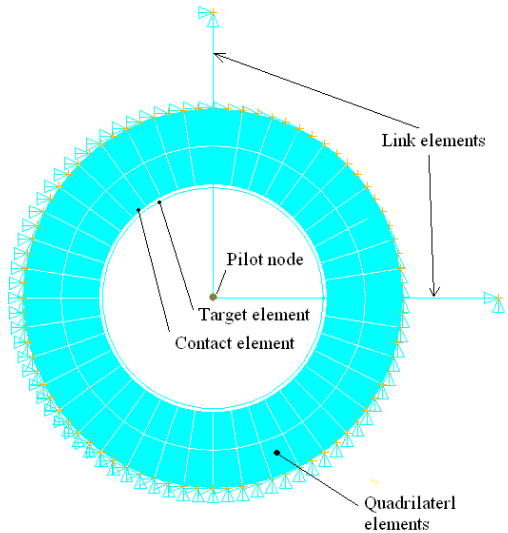


Figure 14 Finite element model used in wear analysis.

The body of the bushing is modeled using 8-node quadrilateral elements. The bushing is constrained along its outer perimeter so that there is no potential for rigid body motion (RBM). The contact between the pin and the bushing is modeled using the

contact-target element pair. The contact elements coat the inner perimeter of the bushing, and a single circular rigid target element is used in place of the pin. The rigid target element is a specialized type of target element that consists of a single node known as the pilot node. The position of the element is determined by the pilot node. This element is constrained from rotation by constraining the rotation on the pilot node. Since translations, depending on the joint forces, are desired in the horizontal and vertical direction, low modulus of elasticity link elements are used to control the motion of the rigid element. The link elements allow the rigid pin to translate but in a manner that prevents RBM. This finite element model configuration is shown in Figure 14.

At each cycle the corresponding slip distance and joint forces can then be used to determine the wear on the bushing according to the wear rule. Once wear on the bushing is computed the geometry is updated. In order to reflect effect of the wear on the kinematics of the mechanism, the kinematic constraints is as updated by changing the variable R_2 (see Section 3.2).

4.3. Comparison between constant and evolving kinematics:

In order to study the effect of the evolving kinematics on the wear at the joint, wear analysis is conducted on two mechanisms; i.e., a mechanism in which the kinematics is assumed to remain constant and a mechanism in which the kinematics changes as the wear evolves. The dimension and mass property for the slider-crank mechanism is shown in Table 1. The bushing used is made of steel with young's modulus 206 GPa and poisons ration 0.29. The value of the wear coefficient used is $1 \times 10^{-8} \text{mm}^3/\text{Nm}$. A total of 23,000 crank cycles is analyzed for wear. The accumulated wear depth at the end of each cycle is recorded for both tests.

Table 1 Dimension and mass properties of the slide-crank mechanism.

	Length (m)	Mass (kg)	Inertia (kg.m ²) $\times 10^{-6}$
Link 1	0.0381	0.4045	204
Link 2	0.1016	0.8175	5500.0
Slider	-	5.54871	-

Figure 15 shows the difference between the accumulated wear depths for both tests. It can be seen from this figure that as the number of cycles increase the difference in wear depth predicted in both conditions increases. It is therefore safe to conclude that the evolving kinematics has an effect on the wear depth predicted.

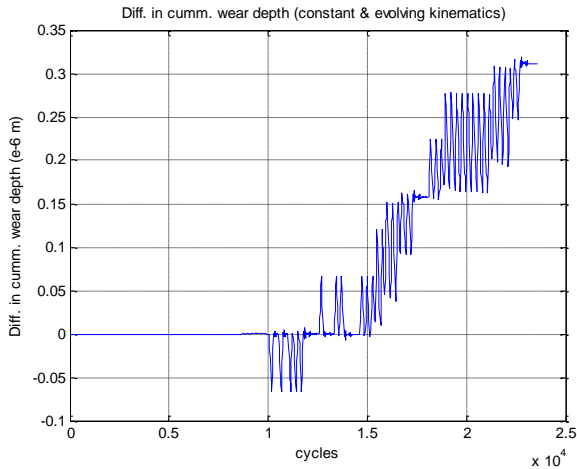


Figure 15 Difference in accumulated wear depth between perfect and imperfect joint.

5. SLIDER-CRANK MECHANISM

An instrumented slider-crank mechanism is used to study the coupling between the wear and evolving kinematics. It will also be used to validating the simulation models being developed. In this section the various aspect of the experimental slider-crank mechanism, including instrumentation and data acquisition will be discussed. Initial results from experimental tests will also be provided.

5.1. Mechanism design

The design of the mechanism is centered around the isolating friction, wear, and error motions to the joint of interest as much as possible. Motion of the crank slider is driven by a high-stiffness block spindle powered by a $\frac{3}{4}$ HP DC motor (Figure 16). The spindle is elevated to the same height as the follower joint to simplify the kinematics. A flywheel (not shown) with 0.0847 kg.m^2 mass moment of inertia is attached to the spindle to help maintain a constant velocity.

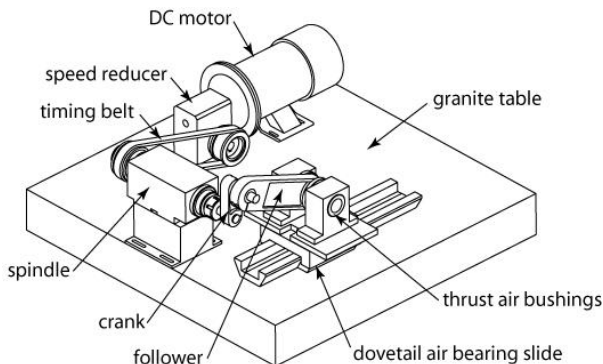


Figure 16 Crank slider mechanism.

The crank and follower arm are both machined from aluminum and pocketed to reduce weight. The crank is clamped to the spindle shaft at one end and to an instrumented pin at the other end. The pin is then free to rotate within a wearing bushing

which is clamped in the follower arm. The follower arm is then constrained to in-plane rotations by two thrust air bushings. These bushings are mounted in pillow blocks which are in turn bolted to a dovetail air bearing stage. Both the thrust bushings and dovetail slide are constructed from porous carbon air bearings to minimize friction and error motions while maintaining a high level of joint stiffness. All of the structural components of the mechanism are bolted to a granite plate.

5.2. Instrumentation

Forces transmitted through the joint of interest are measured via a load cell built into a hardened steel pin (Figure 17). Two full-bridge arrays of strain gages mounted to a necked-down portion of the pin monitor transverse loads while cancelling out bending stresses. The necked portion of the pin, along with a hollow cross section, also serves to localize the strain to the region where the gages are attached. A milled face allows repeatable orientation of the pin with respect to the crank arm. A slip ring mounted to the free end of the pin allows power and signals to be transmitted to and from the strain gages. The load cell is dead-weight calibrated, has a full scale capacity of 400 N and a resolution of 2 N.

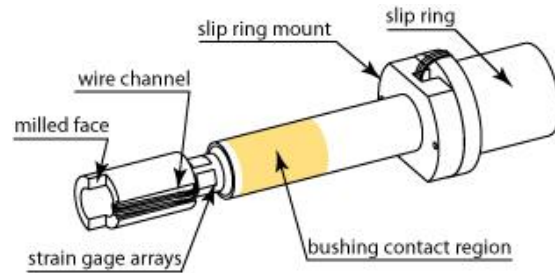


Figure 17 The pin at the joint of interest also serves as a load cell to measure transverse loads during testing.

Simultaneously, two orthogonally mounted capacitance probes monitor the position of the pin relative to bushing (Figure 18). These probes are clamped in aluminum brackets which are bolted to the follower link. Polymer bushings electrically insulate the probes from the brackets. Additionally, the pin, which serves as the target for the probes, is electrically grounded.

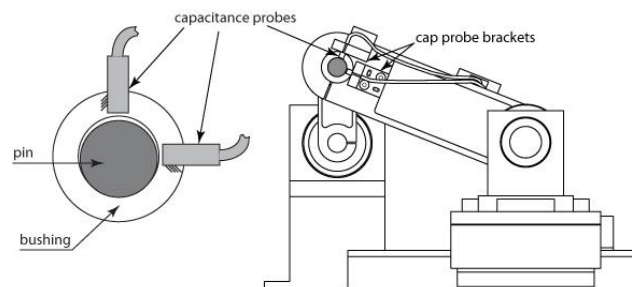


Figure 18 Orthogonally mounted capacitance probes monitor the position of the pin with respect to the bushing.

The angular position of the crank is measured by a hollow shaft incremental encoder attached to the spindle shaft. The encoder has a resolution of 3600 counts per revolution.

5.3. Load Profile

In addition to the inertial loads of the slide and follower arm, the load profile imparted on the pin-bushing joint can be adjusted in two ways (Figure 19). First, a spring can be attached between the air bearing stage and a bracket bolted to the granite plate to provide a positional dependence to the load profile. Also, up to 10 kg of additional mass can be added to the stage. Adding mass to the stage influences the load profile as a function of both crank velocity and position.

5.4. Data acquisition

Data from the load cell, capacitance probe, and encoder are collected simultaneously as waveforms. A packet of data is acquired once per revolution at a pre-specified sampling rate. For each channel, the maximum value, minimum value, and root mean square of the data are then recorded to show broad trends over many cycles at a glance.

Additionally, whole cycles of data from each channel are periodically saved. Force and displacement signals can then be plotted against the crank position to observe the evolution of the force profile and bushing geometry. This also allows events observed in the force data to be directly correlated to events in the displacement data.

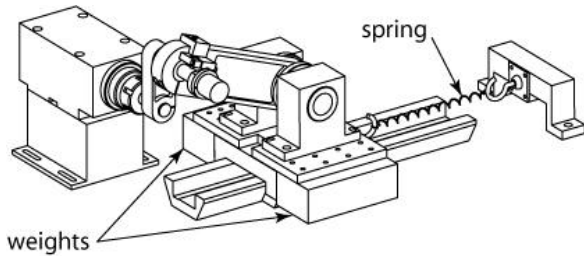


Figure 19 The load profile for the joint of interest can be adjusted by adding mass to the slider stage and by adding a spring between the stage and mechanical ground.

As an initial step of validation, the joint forces from the experiment are compared with that from the dynamic model, as shown in Figure 20. The components of force as well as its magnitude are compared. It turned out the magnitude is well match, while there is a slight phase shift in the components of the force. This shift might be caused by difference in friction model. In addition, the experimental results show oscillation right after the location where two links are aligned. In general, however, two results are well matched for the purpose of wear prediction.

The next step of validation effort is on the comparison of wear profile. As mentioned earlier, wear will occur only at bushing

because it has much higher wear coefficient than that of the pin. Wear results after 21,377 crack cycles is compared in Table 2. Both worn mass and max wear depth from simulation are about 7% less than that from the experiment. Although these results are close, possible explanation of difference is the error in wear coefficient. Schmitz et al. [13] showed that the standard deviation of wear coefficient is more than 10%. Figure 21 shows wear profiles from simulation and experiment.

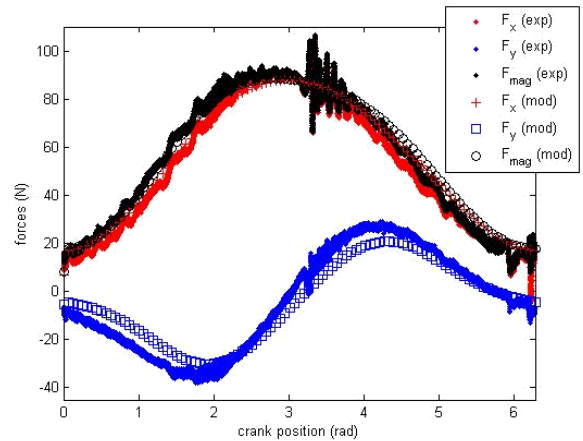


Figure 20 Force magnitude extrema plotted as a function of cycle number. Variations in the cycle maximum force value can be seen to increase as the test progresses.

Table 2 Comparison of wear depth between simulation and wear test

	Experiment	Simulation
Worn area	--	5.5175 mm ²
worn mass	0.1714 g	0.1589 g
Max wear depth	0.4850	0.4524 mm

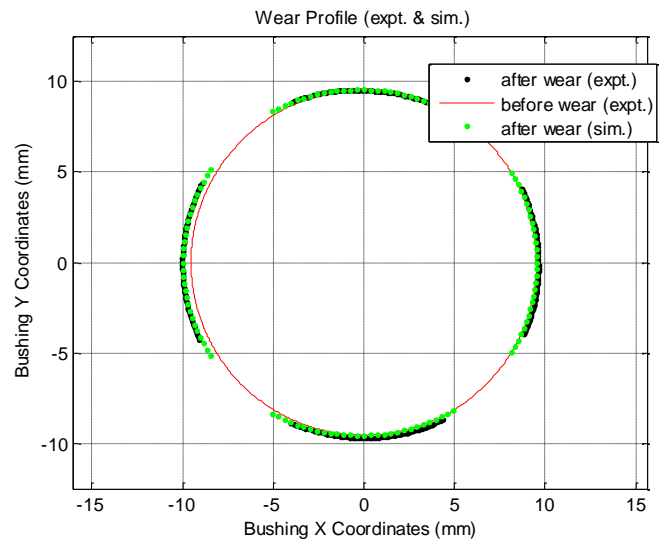


Figure 21 Wear profile comparison between simulation and wear test

CONCLUSIONS

In this work, we showed a simple modeling technique for an imperfect joint and integrated it with wear prediction program. The progress of wear is affected by the change in joint clearance. In the applied slider-crank mechanism, this change in joint clearance accelerates the wear progress because it increases joint force. The joint force in the model has been validated through the measurement of joint force using instrumented pin. The validation of the wear progress is currently being performed.

ACKNOWLEDGMENTS

This research was partly supported by Deere & Company and National Science Foundation (CMMI 0600375). These supports are gratefully acknowledged.

REFERENCES

- [1] S. Dubowsky, On predicting the dynamic effects of clearances in planar mechanisms, *Journal of Engineering for Industry, ASME, Series B96*, 1974, pp. 317-323.
- [2] J. Rhee, A. Akay, Dynamic response of a revolute Joint with clearance, *Mech. Mach. Theory*, Vol. 31, 1996, pp. 121-134
- [3] P. Ravn, A continuous analysis method for planar multibody systems with clearance, *Multibody system dynamics*, Vol. 2, 1998, pp. 1-24.
- [4] A.L. Schwab, J.P. Meijaard, P. Meijers, A comparison of revolute joint clearance models in the dynamic analysis of rigid and elastic mechanical systems, *Mech. Mach. Theory*, Vol. 37, 2002, pp. 895-913.
- [5] J.C. Garcia Orden, Analysis of Joint Clearances in Multibody systems, *Multibody system dynamics*, Vol. 13, 2005, pp 401-420.
- [6] P. Flores, J. Ambrósio, Revolute joints with clearance in multibody systems, *Computers & structures*, Vol. 82, 2004, pp. 1359-1369.
- [7] F. Farahanchi, S.W. Shaw, Chaotic and periodic dynamics of a slider-crank mechanism with slider clearance, *Journal of sound and vibration*, Vol. 177, pp. 307-324.
- [8] S. Dubowsky, F. Freudenstein, Dynamic analysis of mechanical systems with clearances part1: formation of dynamic model, *Journal of Engineering for Industry, ASME*, 1971, pp. 305-309.
- [9] T Furuhashi, N Morita, M Matsuura, Research on dynamics of four-bar linkage with clearance at turning pairs, 1978, *JSME*, Vol. 21 No. 153,
- [10] Design and analysis of multilink flexible mechanisms with multiple clearance connection, *ASME*, 1977, pp. 88-96
- [11] N. H. Kim, D. Won, D. Buris, B. Holtkamp, G. R. Gessel, P. Swanson, W. G. Sawyer, Finite Element Analysis and Validation of Metal/Metal Wear in Oscillatory Contacts, *Wear*, Vol. 258, No. 11-12, pp. 1787-1793, 2005
- [12] S. Mukras, N. H. Kim, W. G. Sawyer, D. B. Jackson and P. Swanson, Design theory and computational modeling tools for systems with wear, paper No. 2007-01-0892, 2007 SAE World Congress, Detroit, MI, April 16-19, 2007
- [13] T. L. Schmitz, J. E. Action, D. L. Burris, J. C. Ziegert, and W. G. Sawyer, Wear-rate uncertainty analysis, *Journal of Tribology*, Vol. 126, pp. 802 - 808, 2004